Journal of Magnetism and Magnetic Materials 420 (2016) 309–316

Contents lists available at ScienceDirect

Journal of Magnetism and Magnetic Materials

journal homepage: www.elsevier.com/locate/jmmm

Crystal growth, structure, magnetic properties and theoretical exchange interaction calculations of Cu_2MnBO_5

S. Sofronova [a], E. Moshkina [a,b], I. Nazarenko [a,*], Yu. Seryotkin [c,d], S.A. Nepijko [e], V. Ksenofontov [f], K. Medjanik [g], A. Veligzhanin [h], L. Bezmaternykh [a]

[a] L.V. Kirensky Institute of Physics, Siberian Branch of Russian Academy of Science, 660036 Krasnoyarsk, Russia
[b] M V Reshetnev Siberian State Aerospace University, 660014 Krasnoyarsk, Russia
[c] V.S. Sobolev Institute of Geology and Mineralogy, SB RAS, 630090 Novosibirsk, Russia
[d] Novosibirsk State University, 630090 Novosibirsk, Russia
[e] Institute of Physics, University of Mainz, 55099 Mainz, Germany
[f] Institute of Inorganic and Analytical Chemistry, University of Mainz, 55099 Mainz, Germany
[g] Lund University, MAX IV Laboratory, 22100 Lund, Sweden
[h] National Research Centre "Kurchatov Institute", 123182 Moscow, Russia

ARTICLE INFO

Article history:
Received 26 April 2016
Received in revised form
15 June 2016
Accepted 13 July 2016
Available online 15 July 2016

Keywords:
Oxyborates
Ludwigites
XMCD
EXAFS
Magnetism

ABSTRACT

Single crystals of ludwigite Cu_2MnBO_5 were synthesized by flux growth technique. The detailed structural and magnetic characterizations of the synthesized samples have been carried out. The cations composition of the studied crystal was determined using X-ray diffraction and EXAFS technique, the resulting composition differ from the content of the initial Mn_2O_3–CuO components of the flux. Magnetic susceptibility measurements and the calculations of the exchange integrals in frameworks of indirect coupling model revealed that monoclinic distortions strongly affect exchange interactions and appearance of magnetic ordering phase at the temperature $T=93$ K. The hypothesis of the existence of several magnetic subsystems was supposed.

1. Introduction

Nowadays, a considerable amount of different type oxyborates (kotoites [1–3], ludwigites [4,5], warwikites [6,7], huntites [8]) is known and studied. The typical feature of these compounds is a presence of quasi-lowdimensional elements – ribbons, ladders, zigzag walls [3–8]. Moreover, metal ions form triangular groups in most compounds, which originates geometric prerequisite for frustrations rising in the system. In these quasi-lowdimensional compounds, a whole range of interesting effects is observed, e.g. charge ordering and two magnetic subsystems existence, which order at different temperatures athwart to each other, in Fe_3BO_5 [9–16]. In $Ni_5GeB_2O_{10}$, significant magnetic susceptibility anisotropy is observed in the paramagnetic region that is extrinsical for divalent Ni ions in octahedral neighbourhood as well as exchange hysteresis loops bias in the small temperature range [17]. For most of these effects, its physical origin reasons are not explored.

The significant magnetic susceptibility anisotropy in the paramagnetic region is mostly observed in compounds which contain so-called Jahn–Teller ions, and it is a consequence of Jahn–Teller effect [18]. It is known that Jahn–Teller effect plays an important role assigning not only structural but also magnetic properties [18].

Among known ludwigites, there are not so many compounds which contain Jahn–Teller ions. In Cu_2FeBO_5 compound, the presence of Jahn-–Teller divalent copper influence structural properties distorting the lattice to monoclinic, however, the magnetic properties are similar to Ni_2FeBO_5 behaviour to a considerable degree [19–21]. In the Ni_2MnBO_5 system, Mn^{+3} Jahn–Teller ion also do not influence significantly structural and magnetic properties of this compound [22,23].

Within the present study we have obtained and investigated structural and magnetic properties of the compound Cu_2MnBO_5 with ludwigite structure, in which one all metallic ions are Jahn–Teller ones: divalent copper and trivalent manganese in octahedral neighbouring. Earlier the preliminary structural and magnetic measurements of one similar ludwigite compound $Cu_{1.5}Mn_{1.5}BO_5$ with the presence of the Mn^{2+} have been carried out [24]. A large magnetic moment and a small magnetic anisotropy, as compared with the others copper and manganese contained ludwigites [23], were detected.

* Corresponding author.

http://dx.doi.org/10.1016/j.jmmm.2016.07.019
0304-8853/

2. Crystal growth

$(Cu,Mn)_3BO_5$ single crystals were synthesized by the flux method with the ratio of the initial components $Bi_2Mo_3O_{12}$:1.3B_2O_3:0.7Na_2CO_3:0.7Mn_2O_3:2.1CuO.

The flux in a mass of 297.5 g was prepared at the temperature $T=1100$ °C in a platinum crucible with the volume of $V=3140$ cm^3 by sequential melting of powder mixtures, first $Bi_2Mo_3O_{12}$ and B_2O_3, then Mn_2O_3 and CuO; finally, Na_2CO_3 was added in portions.

In the prepared flux, the phase crystallizing within a sufficiently wide (about 40 °C) high-temperature range was ludwigite $(Cu,Mn)_3BO_5$. The saturation temperature of the flux was $T_{sat}=865$ °C.

Single crystals of the ludwigite were synthesized by spontaneous nucleation. After homogenization of the flux at $T=1000$ °C for 3 h, the temperature was first rapidly reduced to $(T_{sat}-10)$ °C and then slowly reduced with a rate of 4 °C/day. In 7 days, the growth was completed, the crucible was withdrawn from the furnace, and the flux was poured out. The grown single crystals in the form of prisms with a length of 10 mm and a transverse size of about 2 mm (Fig. 1) were etched in a 20% water solution of nitric acid to remove the flux remainder.

3. The crystal structure

A crystal fragment of $(Cu,Mn)_3BO_5$ was selected for the single-crystal experiment. Diffraction data was collected under room conditions on the Oxford Diffraction Xcalibur Gemini diffractometer (MoKα radiation, 0.5 mm collimator, graphite monochromator) equipped with a CCD-detector. Data reduction including a background correction and Lorentz and polarization corrections was performed with the CrysAlis Pro software. A semi-empirical absorption correction was applied using the multi-scan technique. The unit-cell metrics is monoclinic, space group $P2_1/c$. The structure was solved by the direct methods and refined in the anisotropic approach using SHELX-97 program package [25]. Studied compound is proved to be a monoclinic analogue of $Ni_{2.5}Mn_{0.5}BO_5$ [26]. Crystal data are shown in Table 1. Bond distances of Cu–O are presented in Table 2. The structural data are deposed as CIF at the ICSD (CSD No. 431075). Refinement shows that final chemical formula may be represented as $Cu_{1.43(3)}Mn_{1.57(3)}BO_5$.

In spite of having lower symmetry of $(Cu,Mn)_3BO_5$ – $P2_1/c$ – than common ludwigites have, the main motif of the structure (zigzag walls) remains. Monoclinic distortion springs up because of copper and manganese Jahn–Teller effect. All octahedra around metal ions are characteristically distorted – gaunt in one direction (Table 2).

It is worth to note that in most ludwigites distorted octahedron long axes are located in *bc* plane (Fig. 2b) but in $(Cu,Mn)_3BO_5$ all octahedron long axes have another direction (Fig. 2a), this is probably due to Jahn–Teller effect, which lead to monoclinic distortions and also can influence ions magnetic moment direction.

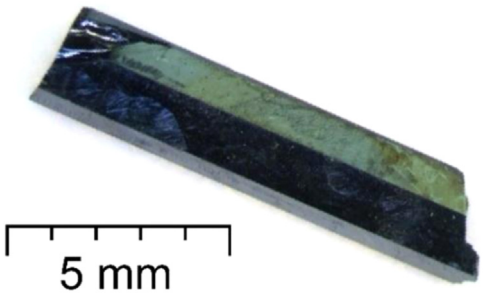

Fig. 1. Optical image of $(Cu,Mn)_3BO_5$ single crystals.

Table 1
The crystal structure parameters of $Cu_{1.43}Mn_{1.57}O_2BO_3$.

Space group, *Z*	$P2_1/c$, 4
a (Å), *b* (Å), *c* (Å), (deg.), V (Å^3)	3.14003(7), 9.3973(2), 12.0242(3), 92.261(2), 354.531(15)
Reflections measured/independent/ with $I>2\sigma(I)/R_{int}$	6461/1186/1070/0.0514
h, *k*, *l*- limits	$-4\le h\le 4$; $-13\le k\le 13$; $-17\le l\le 17$
R1/*wR2*/*Goof* for observed reflections $[I>2\sigma(I)]$	0.0241/0.0541/1.092
R1/*wR2*/*Goof* for all data	0.0291/0.0581/1.092
$\Delta\rho_{max}/\Delta\rho_{min}$ (e/Å^3)	0.938/−0.820

Table 2
Bond length of Me–O for different positions.

Symmetry position	$4e_1$	$4e_2$	$2a$	$2d$
Position distribution of ions	Cu3-0,684% Mn3-0,316%	Cu4-0,01% Mn4-0,99%	Cu2-0,71% Mn2-0,29%	Cu1-0,769% Mn1-0,231%
d(Me–O)	1.9032	1.9067	1.9551	1.9165
	1.9492	1.9081	1.9551	1.9165
	2.0208	2.0098	1.9952	1.9626
	2.0275	2.0103	1.9952	1.9626
	2.3969	2.2084	2.4484	2.6127
	2.5046	2.2813	2.4484	2.6127

Describing ludwigite structure two subsystems are typically picked out – two types of three leg ladders (3LL). The 1st one is formed by triads 4-2-4, the 2nd - by triads 3-1-3. Both 3LL types are presented in the Fig. 3. Particularly, it is related to the fact that the research with neutron diffraction method has shown that Fe_3BO_5 magnetic system split up into two subsystems, each of which one is related to 3LL of types 1 and 2, correspondingly. Typical for $(Cu,Mn)_3BO_5$ monoclinic distortions must affect exchange interactions deeply in 3LL formed by triads 4-2-4. As indicated on the picture, ladders of this type are distorted to a greater extent. Oxygen octahedron long axis is located in triad plane, due to the Jahn–Teller distortion the 2-4 bonds in the triad become nonequivalent, as a consequence, exchange interactions also are different (solid and dashed lines in the Fig. 3), which can extend magnetic lattice. In spite of distortions, such difference is not observed in 3LL of the 2nd type.

In most ludwigites, the strongest exchange interactions occur between 1st type 3LL ions, according to experimental data right in this subsystem magnetic moments ordering takes place firstly. It is confirmed by exchange interaction assessment done for some ludwigites. In the 1st type 3LL, the distances between the ions are the shortest ones. Exchange interactions in the 2nd type 3LL are noticeably weaker. Exchange interactions binding subsystems with each other can be very frustrated because of ions in the structure forming triangular groups.

In Table 2, assumed ions distribution among positions is presented according to the X-ray diffraction data. The position $4e_2$ is entirely occupied by manganese ions, as a rule this position in ludwigite structure is occupied by M^{3+} ions (or multi-valent ions in the ratio with average valence of 3+). Other positions are occupied predominantly by copper ions. However, X-ray diffraction method does not allow to estimate the composition and ions positional distribution with high validity especially if ions have similar electron configuration (e.g. transitional metal ions) therefore

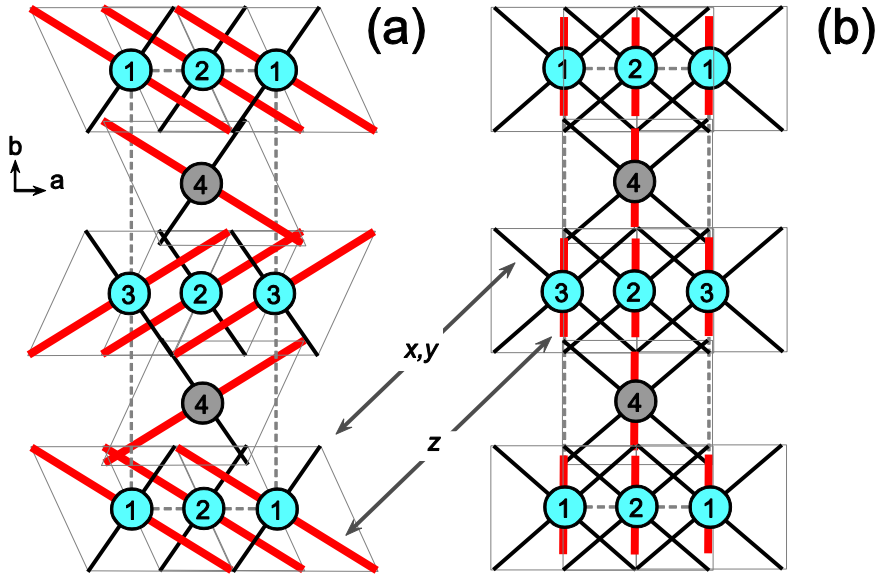

Fig. 2. The octahedra long axis direction changes in $(Cu,Mn)_3BO_5$ (a) and another ludwigites (b). Unit cell side view. Octahedra's axes are shown: *x*, *y* – thin black lines, *z* – thick red lines.

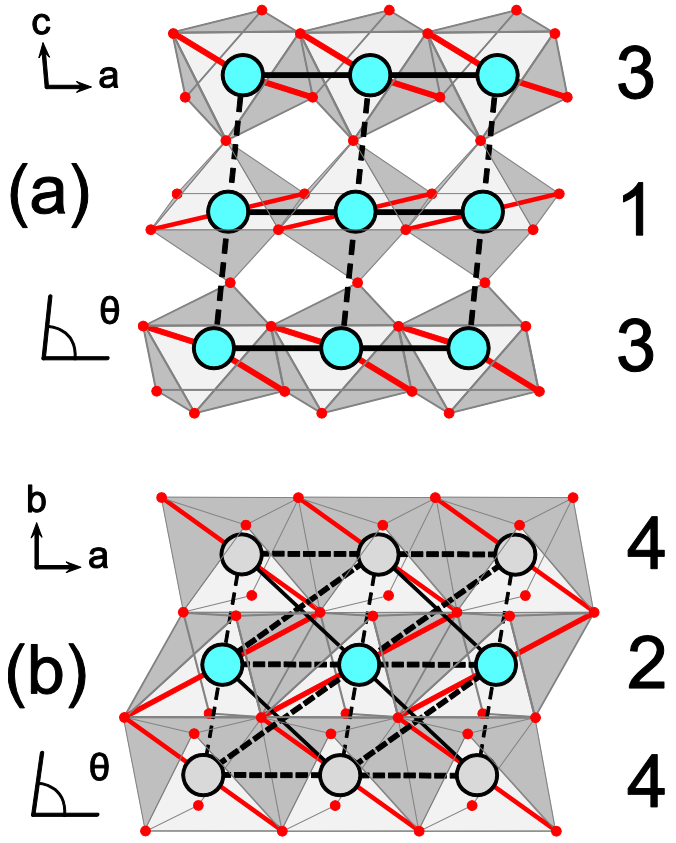

Fig. 3. The distortion of the second (a) and the first (b) type of three leg ladders (3LL). Red lines show long octahedron axis. Black solid and dashed lines show different exchange interactions.

other experimental methods are needed for refinement of composition and copper and manganese ions distribution among positions.

4. EXAFS measurements

The X-ray absorption spectra were measured at the experimental station "Structural material science" of Kurchatov source of synchrotron radiation in Moscow, Russia [27]. The electron energy in a storage ring was 2.5 GeV, the current was about 70 mA. The beam size of the SR (synchrotron radiation) on the sample was 1 mm × 2 mm. The EXAFS spectra were measured by the transmission technique using air ionization chambers. The point measurements of the absorption spectra were carried out in the range of −170–+800 eV relative the energy of *K*-edge of absorption of the base elements – copper (8997 eV) and manganese (6556 eV), which are shown in the Fig. 4a and b, correspondingly. This range was divided into three segments to the measurement time – before the edge region (−170–−20 eV), near-edge region (−20–80 eV) and the EXAFS oscillation region (80–800 eV behind the absorption jump). In the first region the spectrum was measured with the step 10 eV, at near-edge region the step was ~0.5 eV, in the third one the scanning was performed equidistantly with the step 0.05 $Å^{-1}$ of the photoelectron impulses.

Each spectrum was measured in about 20 min. The measurements of every sample spectrum were held 2–3 times and averaged. Processing and analyzing of the results were performed using the program complex IFEFFIT [28,29], version 1.2.11c.

The resultant composition was determined using the jump of the *K*-edge absorption:

$$\frac{N_1}{N_2} = \frac{\Delta(\mu t)_1(\tau\rho)_1 1/M_1}{\Delta(\mu t)_2(\tau\rho)_2 1/M_2}$$

where $\Delta(\mu t)$ – the magnitude of absorption jump; $\tau\rho$ – the product of a single absorption jump length with density; *M* – the element atomic mass. Its values are shown in the Table 3.

The composition of the studied sample was refined by both X-ray diffraction and EXAFS methods. The obtained results are $Cu_{1.43}Mn_{1.57}BO_5$ in the case of the X-ray diffraction and Cu_2MnBO_5 in the case of the EXAFS that quite differ from the content of the initial components Mn_2O_3–CuO (Mn:Cu = 1:1.5). It is supposed that the real composition is close to Cu_2MnBO_5.

The analysis of manganese valence state was performed by the "fingerprint" method. For this purpose, the comparison of the manganese and copper *K*-edge absorption positions of the studied

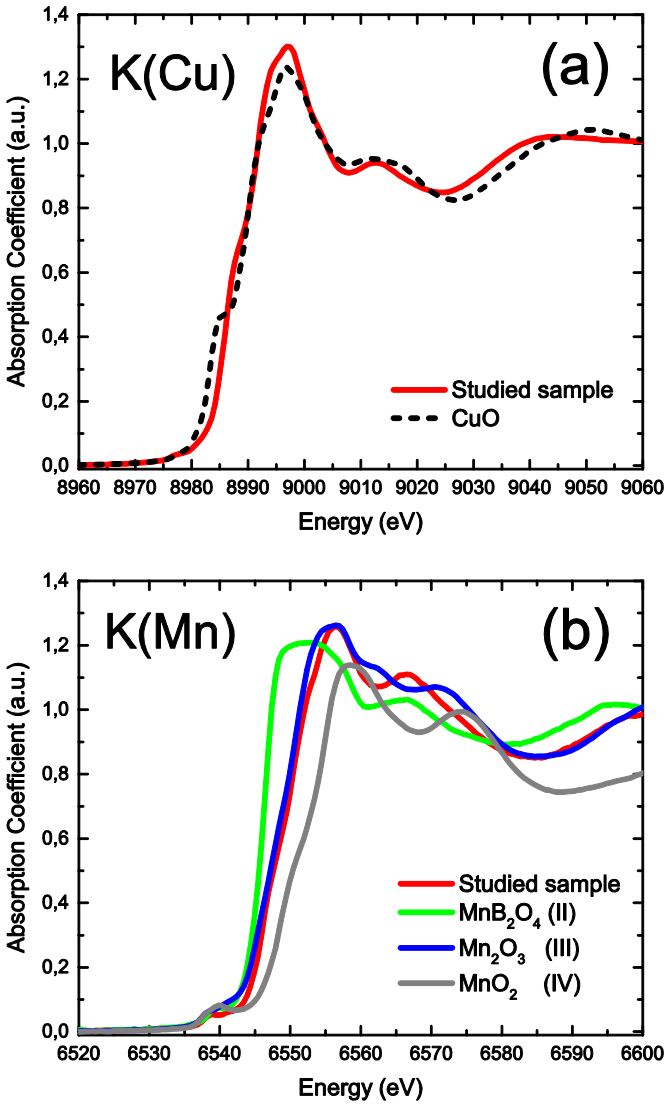

Fig. 4. EXAFS absorption spectra for *K*-edge of Cu (a) and Mn (b).

Table 3
Parameters used for resultant composition calculation.

Element	$\Delta(\mu t)$	ρ	τ	M
Mn	0.778	1	26.0	54.938
Cu	1.094	1	42.4	63.546

sample and the set of characterized and well-studied standards – MnB_2O_4 (Mn^{2+}), Mn_2O_4 (Mn^{3+}) and MnO_2 (Mn^{4+}) – was implemented. As one can see in the Fig. 4, the studied sample position of manganese absorption edge matches the position of Mn_2O_3 absorption edge. The studied sample copper absorption *K*-edge position matches the position of absorption edge of CuO.

Ludwigite structure presume presence of multi-valent ions inasmuch as actual composition is Cu_2MnBO_5, and taking into consideration X-ray diffraction data further we will hold that copper ions occupy positions 1–3 and manganese ions – position 4.

5. Magnetic measurements

Temperature-dependent magnetic susceptibility measurements were carried out with a Quantum-Design MPMS-XL-5 SQUID (superconducting quantum interference device) magnetometer equipped with a 5 T magnet. The powdered sample was immobilized in a closed gelatin capsule. ZFC–FC (zero-field cooled and field cooled) curves (Fig. 5) were acquired over the temperature range 5–350 K with a cooling and heating rate of 1 K min^{-1}, and a magnetic field of either 200 or 2000 Oe. Diamagnetic correction derived from Pascal constants was applied.

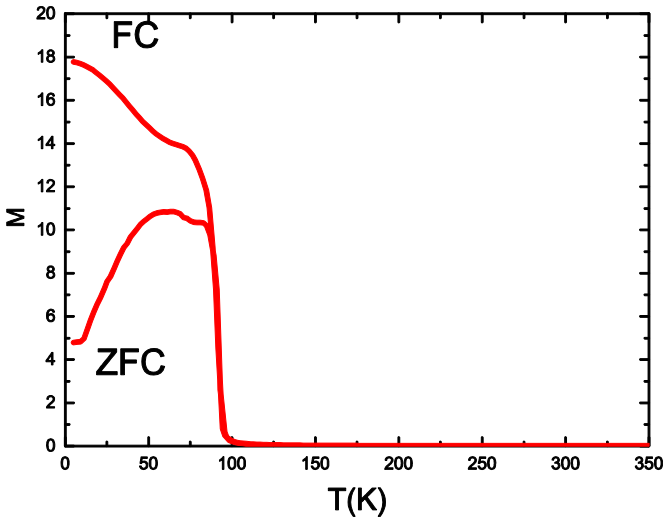

Fig. 5. The temperature-dependent magnetic susceptibility in ZFC and FC regimes.

Magnetic susceptibility curve behavior is typical for ferrimagnetic. Magnetic transition occurs at the temperature of 93 K. In the 75 K region, a feature in the magnetic susceptibility behavior is observed in both ZFC and FC regimes, which can be related to different temperature dependence of magnetization of different sublattices.

In the paramagnetic region, we have used a simple two-sublattice ferrimagnetic model for constants and Curie temperature estimation. From the experimental dependence of inverse susceptibility high temperature region fitting we obtained following parameters: $T_C = -104.2$ K, magnetic moment per unit cell 4.5 μ_B, Curie constants for two sublattices $C = 1.92$ and 0.44. If it is supposed that divalent copper ions form the first sublattice, trivalent manganese ions form the second one, and the compound composition is Cu_2MnBO_5, then theoretical significance of Curie constants are: $C_{Cu} = 0.75$, $C_{Mn} = 3$.

6. XMCD measurements

Our experiment has been performed at MAX II storage ring (beamline I1011) in Lund, Sweden [29]. All measurements were done at “octupole” endstation in total electron yield mode. Variation of magnetic field during an experiment was possible up to 0.8 T. Beamline I1011 [30] is a soft X-ray beamline, covering the energy range from 120 to 2000 eV, with an energy resolving power of around $E/dE = 5000$ at the lowest used photon energies. It's equipped with a collimated plane grating monochromator and an elliptically polarizing undulator, providing almost 100% linearly and circularly polarized radiation. This makes X-ray magnetic circular dichroism (XMCD) technically feasible. The sample was placed on the keypad allowing to change the angle of incidence of synchrotron radiation to the sample in the equatorial and azimuthal planes. The equatorial angle varies in the range of $\theta = 22$–158°. In our measurements the azimuth angle is $\phi = 90°$. The sample holder was being cooled with liquid nitrogen, which allowed to carry out measurements in the 300–100 K temperature range. The vacuum in the sample chamber was of the 10^{-10} mbar

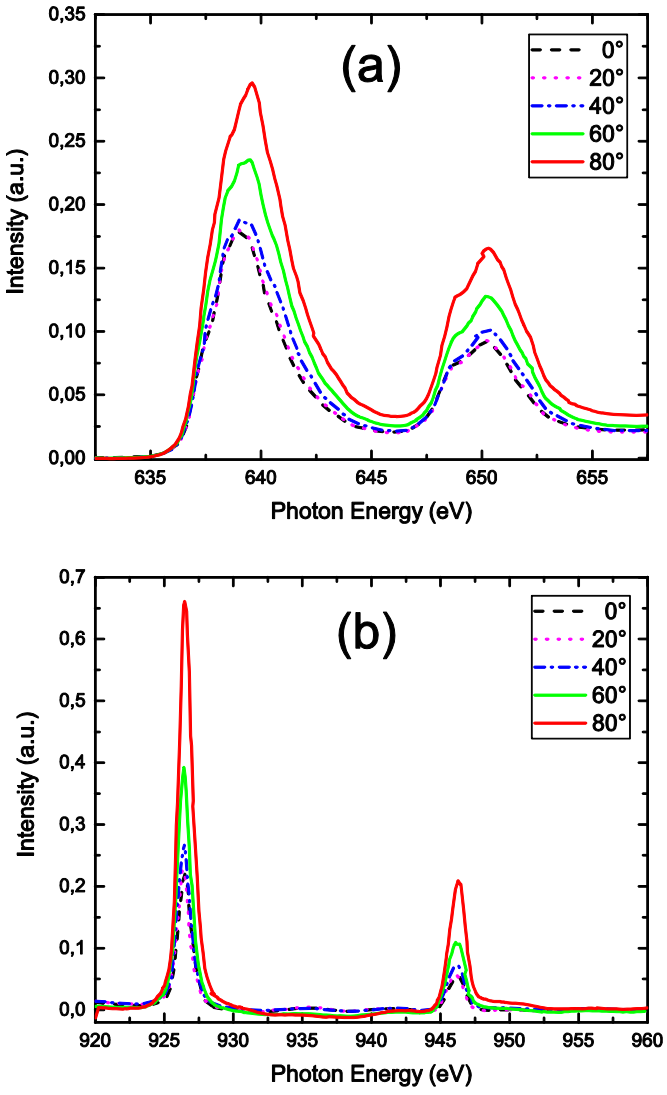

Fig. 6. The $L_{2,3}$-edge of absorption of Mn (a) and of Cu (b).

order.

The samples had the shape of a needle, a long direction of the single crystal is an a crystallographic direction and the other two crystallographic directions for the study of single crystals were not specified. Equatorial angle was varied in increments of 20° to the possible extent. Samples were fixed so that a change in the equatorial angle corresponded to a change of the beam direction with respect to the crystallographic *a* axis.

Fig. 6a and b show the angular dependence of the L_2, L_3 manganese and copper ions absorption spectra. As can be seen from the figure, there is a strong angular dependence at the minimum angle between the beam and the crystallographic *a* axis, and the most intense spectra that most likely indicates that the magnetic moments of the ions have a projection on the a axis. In ludwigites, which were previously studied for orientational dependence of the magnetic structure, the magnetic moments of the ions are in the *bc* plane [9]. Perhaps, the Jahn–Teller effect leads not only to a distortion of the crystal structure but also to a change in the direction of the magnetic moments of the ions.

Received XMCD signals measured at 90° to the crystallographic a axis, both for copper and manganese vary slightly with temperature. Most likely, this behavior may be due to the fact that the measurements were performed in a direction perpendicular to the magnetic moments of the copper and manganese ions. Based on these results, it can be assumed that the magnetic moments of copper and manganese ions are in the same plane and have a projection on the crystallographic a axis. To verify the temperature behavior of the copper and manganese ions magnetization, further research is needed in other areas with larger oriented single crystal.

7. Group-theoretical analysis of possible magnetic structures

Possible magnetic structures were determined using the group-theoretical analysis [31]. The expansion of the magnetic representation by irreducible representations for the center of the Brillouin zone was obtained:

$$d_{k=0} = 6\tau_1 + 12\tau_2 + 6\tau_3 + 12\tau_4$$

The expansion of the magnetic representation by irreducible representations for atoms in different positions are

$$d_{k=0}(2a) = 3\tau_2 + 3\tau_4$$
$$d_{k=0}(2d) = 3\tau_2 + 3\tau_4$$
$$d_{k=0}(4e_{1,2}) = 3\tau_1 + 3\tau_2 + 3\tau_3 + 3\tau_4$$

Then the basis vectors were built (Table 4), which define the direction of the magnetic moments of ions for each irreducible representation τ: τ_1, τ_3 irreducible representations are magnetic not for all crystallographic positions with the exception of 2*a*, 2*d* positions. For other positions these representations provide an antiferromagnetic (AFM) structure. The irreducible representation τ_2 gives ferromagnetic (ferrimagnetic) structure along the axis *y*, while τ_4 gives ferromagnetic (ferrimagnetic) structure in the *xz* plane. If we assume that the magnetic cell coincides with the crystallographic, then based on the results of XMCD research, magnetic phase transition is most likely related to the irreducible representation of the τ_4.

8. Indirect coupling model

To analyze the magnetic structures and estimate the super-exchange interactions in Cu_2MnBO_5 crystal, we used a simple indirect coupling model [32] based on the theory of the super-exchange interaction of Anderson [34] and Zavadskii [33] and Eremin [35]. Within the indirect coupling model, the structure of the

Table 4
Basis vectors defining the direction of the magnetic moments of ions for each irreducible representation.

Pos.	#	τ_1	τ_2	τ_3	τ_4
2*a*	1		*x,y,z*		*x,y,z*
	2		$-x,y,-z$		$x,-y,z$
2*d*	3		*x,y,z*		*x,y,z*
	4		$-x,y,-z$		$x,-y,z$
$4e_1$	5	*x,y,z*	*x,y,z*	*x,y,z*	*x,y,z*
	6	$-x,-y,-z$	*x,y,z*	$-x,-y,-z$	*x,y,z*
	7	$-x,y,-z$	$-x,y,-z$	$x,-y,z$	$x,-y,z$
	8	$x,-y,z$	$-x,y,-z$	$-x,y,-z$	$x,-y,z$
$4e_2$	9	*x,y,z*	*x,y,z*	*x,y,z*	*x,y,z*
	10	$-x,-y,-z$	*x,y,z*	$-x,-y,-z$	*x,y,z*
	11	$-x,y,-z$	$-x,y,-z$	$x,-y,z$	$x,-y,z$
	12	$x,-y,z$	$-x,y,-z$	$-x,y,-z$	$x,-y,z$

Table 5
The calculated value of superexchange integrals.

Crystallographic positions of interacting magnetic ions	The angles of the indirect coupling between magnetic ions	The superexchange integrals	The value of superexchange integrals, K
1-1	$\alpha=\beta=89°$	$J_{ij}^{90°}=bcJ_{Cu}(\sin\alpha+\sin\beta)$	7.890
2-2	$\alpha=\beta=86°$		7.872
3-3	$\alpha=89°$, $\beta=87°$		7.885
4-4	$\alpha=99°$, $\beta=96°$	$J_{ij}^{90°}=\frac{c}{16}\left(bJ_{Mn}-2\left(c+\frac{5}{3}b\right)U_{Mn}\right)(\sin\alpha+\sin\beta)$	−5.459
1-3	$\alpha=120°$	$J_{ij}^{90°}=2bcJ_{Cu}\sin\alpha$	6.834
1-4	$\alpha=99°$, $\beta=91°$	$J_{ij}^{90°}=\frac{c}{4}\left[-b(U_{Cu}+U_{Mn})\sin\alpha+J_{Cu}\left(c+\frac{5}{3}b\right)(\sin\alpha+\sin\beta)\right]$	0.122
1-4	$\alpha=99°$, $\beta=93°$	$J_{ij}^{90°}=\frac{c}{4}\left[-b(U_{Cu}+U_{Mn})+J_{Cu}\left(c+\frac{2}{3}b\right)\right](\sin\alpha+\sin\beta)$	−6.012
2-3	$\alpha=99°$, $\beta=95°$	$J_{ij}^{90°}=2bcJ_{Cu}(\sin\alpha+\sin\beta)$	15.656
2-3	$\alpha=89°$, $\beta=92°$	$J_{ij}^{90°}=bcJ_{Cu}(\sin\alpha+\sin\beta)$	7.888
2-4	$\alpha=98°$, $\beta=73°$	$J_{ij}^{90°}=\frac{c}{4}\left[\left(J_{Cu}\left(\frac{2}{3}b+c\right)-b(U_{Cu}+U_{Mn})+\right)\sin\alpha+J_{Cu}\left(\frac{8}{3}b+c\right)\sin\beta\right]$	−0.010
2-4	$\alpha=154°$	$J_{ij}^{180°}=\left(-\frac{1}{3}b^2(U_{Cu}+U_{Mn})+\left(\fr\frac{1}{9}b^2+\frac{1}{2}c^2\right)J_{Cu}\right)\lvert\cos\alpha\rvert$	−8.339
2-4	$\alpha=162°$	$J_{ij}^{180°}=\left(\frac{1}{9}b^2+\frac{1}{2}c^2\right)J_{Cu}\lvert\cos\alpha\rvert$	1.772
3-4	$\alpha=89°$, $\beta=106°$	$J_{ij}^{90°}=\frac{c}{4}\left[J_{Cu}\left(\frac{5}{3}b+c\right)\sin\alpha+\left(J_{Cu}\left(\frac{2}{3}b+c\right)-b(U_{Cu}+U_{Mn})\right)\sin\beta\right]$	−0.773
3-4	$\alpha=95°$, $\beta=101°$	$J_{ij}^{90°}=\frac{c}{4}\left[\left(J_{Cu}\left(\frac{5}{3}b+c\right)-b(U_{Cu}+U_{Mn})\right)\sin\alpha+\left(J_{Cu}\left(\frac{2}{3}b+c\right)-b(U_{Cu}+U_{Mn})\right)\sin\beta\right]$	−5.004
3-4	$\alpha=116°$	$J_{ij}^{90°}=\frac{c}{4}\left(J_{Cu}\left(\frac{2}{3}b+c\right)-b(U_{Cu}+U_{Mn})\right)\sin\alpha$	−2.721
3-4	$\alpha=118°$	$J_{ij}^{90°}=\frac{c}{4}\left(J_{Cu}\left(\frac{5}{3}b+c\right)-b(U_{Cu}+U_{Mn})\right)\sin\alpha$	−1.802

crystals can be characterized by the following integrals of the indirect exchange coupling with regard to occupations of individual cation orbitals and symmetries of the lattice of indirect couplings $J_{ij}^{\alpha\beta}$, where i and j are the numbers of nonequivalent crystallographic positions for magnetic ions and α, β are the angles of the indirect coupling between magnetic ions.

The calculated exchange integrals for Cu_2MnBO_5 are presented in the Table 5.

Here, b and c are the electron transfer parameters being squares of ligand–cation intermixing coefficients for the σ and π coupling, respectively (the values of these parameters are $b=0.02$ and $c=0.01$); U (Cu^{2+})=2.2 eV and U (Mn^{3+})=5 eV are the cation-ligand excitation energies; J^{in} (Cu^{2+})=1.7 eV and; J^{in} (Mn^{3+})=2.68 eV are the integrals of the interatomic exchange interaction [32].

In Cu_2MnBO_5 octahedra are distorted, and their z axes are not in the bc-plane as in other ludwigites, e.g. Co_3BO_5 or Fe_3BO_5, etc. Due this distortion, superexchange interactions occur via these z-axes, and not via x- y-axes as in noted above compounds (See Fig. 2).

Using constants calculated in the framework of the indirect exchange interaction model we evaluated the energy of all possible magnetic structures in case of the magnetic cell coincided with the crystallographic one. We have considered cases where the magnetic atoms are arranged ferromagnetic, ferrimagnetic, antiferromagnetic along one of the components (x, y or z). We cannot distinguish any direction inasmuch as in our approach we consider isotropic exchange interactions. Various structures energies are shown in the Table 6. As can be seen from the table, the ferromagnetic structures are energetically more favorable. The most energetically favorable magnetic structure is shown in the Fig. 7.

As noted above, in the iron ludwigite magnetic structure is divided into two subsystems - three-legged ladders, which in our case are distorted because of the Jahn–Teller effect. This leads to

Table 6
Energies of different magnetically ordered structures for the case $\vec{k}$=0.

Title	2a	2d	$4e_1$	$4e_2$	E, eV
FIM1	↑↑	↑↑	↑↑↑↑	↓↓↓↓	−0.06636
FIM2	↓↓	↑↑	↑↑↑↑	↓↓↓↓	−0.04909
AFM1	↑↓	↑↓	↑↓↑↓	↓↑↓↑	−0.03881
FIM3	↑↑	↓↓	↓↓↓↓	↓↓↓↓	−0.02901
FM	↑↑	↑↑	↑↑↑↑	↑↑↑↑	−0.01380
FIM4	↓↑	↑↑	↓↑↓↑	↓↓↓↓	−0.01216
FIM5	↑↑	↑↑	↓↑↓↑	↓↑↓↑	−0.00480
FIM6	↑↑	↓↓	↑↑↑↑	↓↓↓↓	0.00764
AFM2	↓↑	↑↓	↓↑↓↑	↓↑↓↑	0.01449
AFM3	↓↑	↓↑	↑↓↑↓	↓↑↓↑	0.01998
FIM7	↑↑	↑↑	↓↓↓↓	↑↑↑↑	0.02491
FIM8	↑↑	↑↑	↓↓↓↓	↓↓↓↓	0.02683
FIM9	↑↓	↑↑	↓↓↓↓	↓↓↓↓	0.03444
FIM10	↑↑	↓↓	↑↑↑↑	↑↑↑↑	0.04204

the fact that the exchange interactions among the right and the left neighbours in the first type ladder are different, which may lead to a doubling of the magnetic cell. Let us consider the exchange interactions in the three-legged ladders of both types in more detail. The Fig. 8 shows the exchange interactions inside ladders of each type as well as provides the exchange interaction between the stairs through the ions 1 and 3. As can be seen from the figure, a 90-degree exchange interactions between ions 2 and 4 are equal to 0, correspondingly, a decisive role will be played by 180° exchange interactions, which are different for the right and left neighbours not only in magnitude but also in sign: −8.3 and 1.8 K, correspondingly. Moreover, the exchange interaction between Mn ions in position 4 is antiferromagnetic that can also lead to a doubling of the magnetic cell along the c axis. In the second type ladder, 90-degree exchange interactions between the ions 1 and 3 are also very weak and apparently the direction of the magnetic moments of ions 1 and 3 will depend on the ordering of

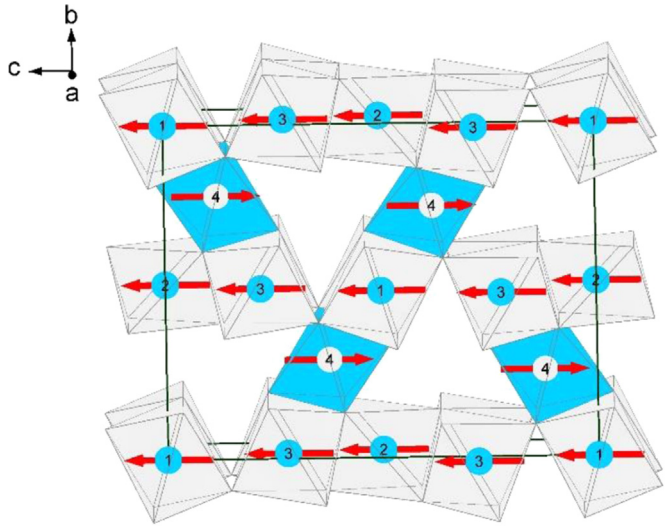

Fig. 7. The proposed magnetic structure of Cu_2MnBO_5.

ions 2 and 4. If the magnetic moments in positions 2 and 4 are arranged antiferromagnetic along the *a* axis, there is a strong competition for exchange interactions in position 3. The exchange interaction between the ions 4 and 1 is also different for the nearest two neighbours.

Since the exchange interactions are unbalanced and there is a competition between the exchange interactions, we evaluated a number of different energy duplicated cells. The Table 7 shows the values of exchange energy per one formula unit. If you compare it with the results from the Table 6, it will be obvious that the doubling of the unit cell is less favourable energetically.

Table 7
Energies of different magnetically ordered structures for the case $\vec{k}=\pi/\vec{a}$.

Type	2*a*	2*d*	$4e_1$	$4e_2$	$2a'$	$2d'$	$4e_1'$	$4e_2'$	*E*, eV
1	↑↑	↑↑	↑↑↑↑	↓↑↓↑	↑↑	↑↑	↑↑↑↑	↑↓↑↓	−0.04761
2	↓↓	↑↑	↑↑↑↑	↑↓↑↓	↓↓	↑↑	↑↑↑↑	↓↑↓↑	−0.04658
3	↓↓	↓↑	↓↓↓↓	↑↑↑↑	↓↓	↑↓	↓↓↓↓	↑↑↑↑	−0.02394
4	↑↑	↓↑	↑↑↑↑	↓↑↓↑	↑↑	↑↓	↑↑↑↑	↑↓↑↓	−0.02394
5	↑↓	↑↑	↑↑↑↑	↑↑↑↑	↓↑	↑↑	↑↑↑↑	↑↑↑↑	−0.01596
6	↑↑	↓↑	↑↑↑↑	↓↑↓↑	↑↑	↑↓	↑↑↑↑	↑↓↑↓	−0.01423
7	↓↑	↑↓	↓↓↓↓	↑↓↑↓	↑↓	↓↑	↓↓↓↓	↓↑↓↑	−0.00828
8	↓↓	↓↑	↓↓↓↓	↑↓↑↓	↓↓	↑↓	↓↓↓↓	↓↑↓↑	−0.00521
9	↓↓	↓↑	↑↑↑↑	↑↓↑↓	↓↓	↑↓	↑↑↑↑	↓↑↓↑	−0.00418
10	↑↑	↓↓	↑↓↑↓	↑↓↑↓	↑↑	↓↓	↓↑↓↑	↓↑↓↑	−0.00376
11	↑↓	↓↓	↓↑↓↑	↑↓↑↓	↓↑	↓↓	↑↓↑↓	↓↑↓↑	0.00219

Based on our estimates, we can assume that in this compound the magnetic cell coincides with the crystallographic one, the magnetic structure is ferrimagnetic and associated with irreducible representation τ_4. It is possible that in order to reduce competition between the exchange interactions as well as in iron ludwigite different magnetic subsystems will be ordered perpendicular to each other.

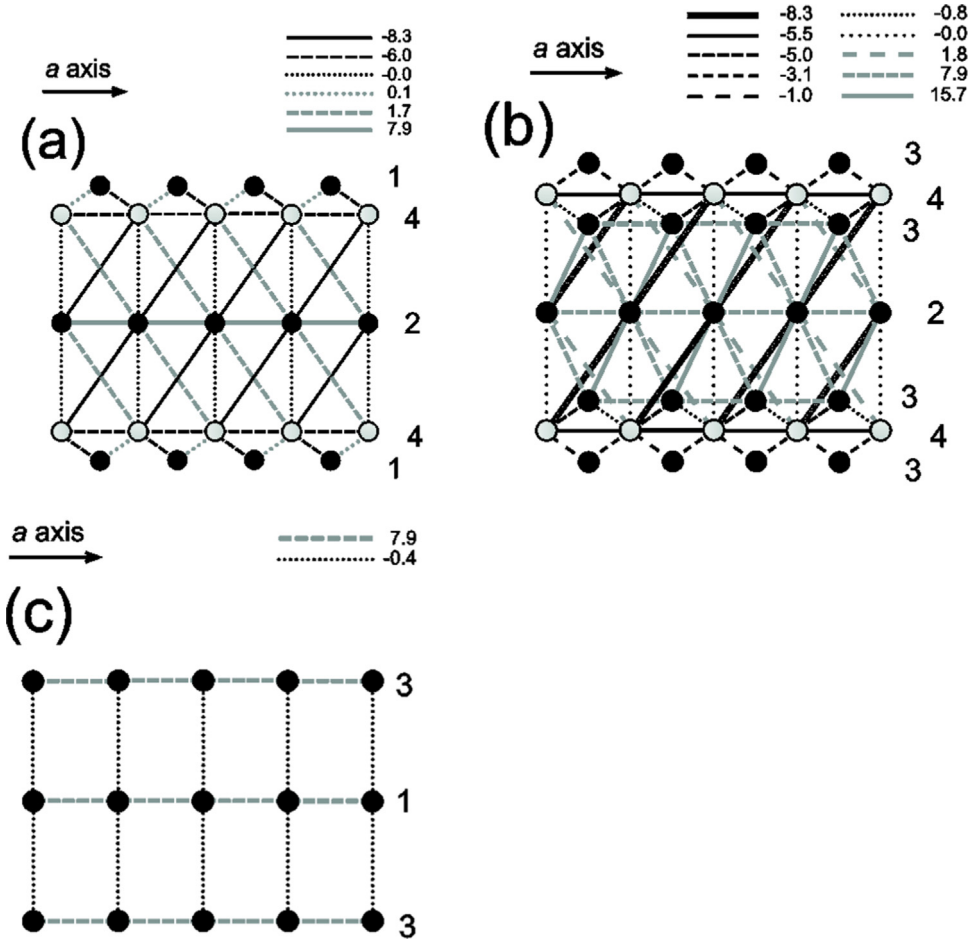

Fig. 8. Exchange interactions in both types 3LLf. (a) – Exchange interactions in the first type 3LL and connection with ion in position 1; (b) – Exchange interactions in the first type 3LL and connection with ion in position 3; (c) – Exchange interactions in the second type 3LL.

9. Conclusions

X-ray absorption spectra and X-ray diffraction study allowed to determine the structure, the ions coordinates, clarify the composition and distribution of ions among the positions. Monoclinic distortions caused by the Jahn–Teller effect of divalent copper and trivalent manganese lead to the fact that, in contrast to all investigated currently monocrystalline ludwigites, in Cu_2MnBO_5 atoms magnetic moments lie in one plane extending along the *a* axis whereas in Fe_3BO_5, Co_3BO_5, the magnetic moments of the ions are located in the *bc* plane.

Calculation of the exchange interactions has shown that in the system there is a competition of exchange interactions, and some exchange interactions are close to zero. In our proposed structure there are magnetic frustrating interactions that can lead to the decomposition into subsystems. The presence of almost zero interactions can lead to the fact that one of the sublattices or subsystems will be weakly related to the rest ones, or not fully ordered. Marginally, this is confirmed by the behaviour of the magnetization - in the 75–80 K region on the magnetization curves, a feature is observed that is associated with the presence of different temperature dependences of different sublattices magnetization. Perhaps, one of the sublattices (associated with the position 1) is weakly related or completely disordered due to frustrated bonds that leads to magnetization dependencies thermal hysteresis.

Acknowledgments

X-ray diffraction experiment was carried out at the Centre on Molecular Design and Ecologically Safe Technologies at the Novosibirsk State University. The reported study was funded by Russian Foundation for Basic Research (RFBR) and Government of Krasnoyarsk Territory according to the research project No. 16-42-243028.

References

[1] R.E. Newnham, M.J. Redman, R.P. Santoro, Z. Krist. 121 (1965) 418.
[2] R.E. Newnham, R.P. Santoro, P.F. Seal, G.R. Sallings, Phys. status solidi 16 (1966) K17.
[3] L.N. Bezmaternykh, S.N. Sofronova, N.V. Volkov, E.V. Eremin, O.A. Bayukov, I. I. Nazarenko, D.A. Velikanov, Physica status solidi B 249 (8) (2012) 1628–1633.
[4] E. Bertaut, Acta Crystollogr. 3 (1950) 473.
[5] H. Neuendorf, W. Gunser, JMMM 173 (1997) 117.
[6] J.C. Fernandes, R.B. Guimarães, M.A. Continentino, H.A. Borges, J.V. Valarelli, Alex Lacerda, Phys. Rev. B 50 (1994) 16754.
[7] A. Arauzo, N.V. Kazak, N.B. Ivanova, M.S. Platunov, Y.V. Knyazev, O.A. Bayukov, L.N. Bezmaternykh, I.S. Lyubutin, K.V. Frolov, S.G. Ovchinnikov, J. Bartolomé, JMMM 392 (2015) 114–125.
[8] A.M. Kadomtseva, Yu. F. Popov, G.P. Vorob'ev, A.P. Pyatakov, S.S. Krotov, K. I. Kamilov, V. Yu Ivanov, A.A. Mukhin, A.K. Zvezdin, A.M. Kuz'menko, L. N. Bezmaternykh, I.A. Gudim, V.L. Temerov, Low Temp. Phys. 36 (2010) 511.
[9] P. Bordet, E. Suard, Phys. Rev. B 79 (2009) 144408.
[10] J. Larrea J, D.R. Sánchez, F.J. Litterst, E.M. Baggio-Saitovitch, J.C. Fernandes, R. B. Guimaraes, M.A. Continentino, Phys. Rev. B 70 (2004) 174452.
[11] A. Latgé, M.A. Continentino, Phys. Rev. B 66 (2002) 094113.
[12] J.C. Fernandes, R.B. Guimarães, M.A. Continentino, L. Ghivelder, R.S. Freitas, Phys. Rev. B 61 (2) (2000) R850.
[13] J. Bartolome, A. Arauzo, N.V. Kazak, N.B. Ivanova, S.G. Ovchinnikov, Yu. V. Knyazev, I.S. Lyubutin, Phys. Rev. B 83 (2011) 144426.
[14] E. Vallejo, M. Avignon, JMMM 310 (2007) 1130–1132.
[15] M.-H. Whangbo, H.-J. Koo, J. Dumas, M.A. Continentino, Inorg. Chem. 41 (8) (2002) 2193.
[16] M. Matos, J. Terra, D.E. Ellis, A.S. Pimentel, JMMM 374 (2015) 148–152.
[17] S.N. Sofronova, L.N. Bezmaternykh, E.V. Eremin, I.I. Nazarenko, N.V. Volkov, A. V. Kartashev, E.M. Moshkina, JMMM 401 (2016) 217–222.
[18] K.I. Kugel, D.I. Khomskii, Uspekhi Fizicheskikh Nauk, 25, 1982, pp. 231–256.
[19] J.C. Fernandes, R.B. Guimarães, M.A. Continentino, H.A. Borges, A. Sulpice, J.-L. Tholence, J.L. Siqueira, L.I. Zawislak, J.B.M. da Cunha, C.A. dos Santos, Phys. Rev. B 58 (1) (1998) 287.
[20] M.A. Continentino, J.C. Fernandes, R.B. Guimaraes, H.A. Borges, A. Sulpice, J.-L. Tholence, J.L. Siqueira, J.B.M. da Cunha, C.A. dos Santos, Eur. Phys. J. B 9 (1999) 613–618.
[21] G.A. Petrakovskiia, b, L.N. Bezmaternykha, D.A. Velikanova, A.M. Vorotynova, *, O.A. Bayukova, b, M. Schneider, Phys. Solid State 51 (10) (2009) 2077–2083.
[22] E. Moshkina, S. Sofronova, A. Veligzhanin, M. Molokeev, I. Nazarenko, E. Eremin, L. Bezmaternykh, JMMM 402 (2016) 69–75.
[23] L.N. Bezmaternykh, E.M. Kolesnikova, E.V. Eremin, S.N. Sofronova, N.V. Volkov, M.S. Molokeev, JMMM 364 (2014) 55–59.
[24] L. Bezmaternykh, E. Moshkina, E. Eremin, M. Molokeev, N. Volkov, Y. Seryotkin, SSP 233-234 (2015) 133–136.
[25] G.M. Sheldrick, Acta Cryst. A 64 (2008) 112–122.
[26] K. Bluhm, H. Mueller Buschbaum, Z. Anorg. Allg. Chem. 579 (1989) 111–115.
[27] A.A. Chernyshov, A.A. Veligzhaninand, Y.V. Zubavichus, Nucl. Instrum. Methods Phys. Res. Sect. A: Accel. Spectrom. Detect. Assoc. Equip. 603 (2009) 95–98.
[28] M. Newville, J. Synchrotron Radiat. 8 (2001) 322–324.
[29] B. Ravel, M. Newville, J. Synchrotron Radiat. 12 (2005) 537–541.
[30] I.A. Kowalik, G. Öhrwall, B.N. Jensen, R. Sankari, E. Wallén, U. Johansson, O. Karis, D. Arvanitis, J. Phys. Conf. Ser. 211 (2010) 012030.
[31] Yu. A. Izyumov, R.P. Ozerov, Magnetic Neutron Diffraction, Plenum Press, N.Y. 1979, p. 598.
[32] O.A. Bayukov, A.F. Savitskii, Phys. Status Solidi B 155 (1989) 249.
[33] O.A. Bayukov, A.F. Savitskii, Fiz. Tverd. Tela 36 (1994) 1923.
[34] P.W. Anderson, Phys. Rev. 115 (1959) 2.
[35] M.V. Eremin, Fiz. Tverd. Tela 24 (1982) 423.